

Acoustic Emission Geomechanics and Seismic Energy Budgets of Laboratory Hydraulic Fracturing

Shawn C. Maxwell (IMaGE), Sebastian Goodfellow (DGI GeoScience) and R. Paul Young (University of Toronto)

Summary

A laboratory experiment was performed to characterize a hydraulic fracture created in rock samples subjected to various stress states. Hydraulic fracture geometries were determined using a μ CT scan and compared to recorded acoustic emissions (AE) with moment magnitudes smaller than -7. The experiment found that more planar fracture geometries were created at higher levels of differential stress, and that the associated number of AE was reduced. Geomechanical modeling of the hydraulic fracturing surfaces was able to reproduce similar fracture geometries, and the model estimated AE were consistent with the AE observations. Energy budgets were also compared between the total energy associated with injection, total sample strain and AE. The AE represent a small portion of the total energy, consistent with the portion detected in field microseismic monitoring. The laboratory hydraulic fracturing provides a controlled setting to understand the influence of geomechanical factors controlling fracture networks, providing a unique opportunity to understand the context of passive seismic observations.

Introduction

Microseismic observation of hydraulic fractures in unconventional reservoirs has highlighted the importance of reservoir conditions and geological heterogeneity on hydraulic fracture network geometries. Passively recorded microseismicity provides insights into the fracture growth, often leading to interpretations about the geomechanical response of the reservoir. Nevertheless, quantitative microseismic interpretation is often challenging, due to limited reservoir characterization of the geomechanical and geologic settings including initial stresses and pre-existing fractures. Seldom is there specific knowledge of the exact hydraulic fracture geometry other than inferences from recorded microseismicity.

In contrast, hydraulic fracturing in the laboratory can be used to characterize the fracture geometry resulting from different conditions (e.g. stress state). The resulting fracture geometry can then be directly determined. Similar to microseismicity recorded in the field, acoustic emissions (AE) can also be monitored using sensitive, high-frequency acquisition systems. However, it is important to consider the differences between laboratory AE and field microseismicity (e.g. Goodfellow et al., 2015). AE are much higher frequency (typically MHz signals) associated with sources with spatial dimensions of the order of millimeters. Calibrated AE acquisition can be used to estimate moment magnitudes of the order of -7. Scaling differences are therefore important between AE and field microseismicity, particularly in terms of potential differences in source mechanisms. Nevertheless, laboratory hydraulic fracturing can be used to compare passive 'seismic' sources with a controlled hydraulic fracture.

In this paper, we present laboratory observations of hydraulic fractures created at different differential stresses, to explore the resulting fracture geometries and associated AE. The fractures and associated AE are compared with the results from a geomechanical model of hydraulic fracture growth under the same conditions. The energy portion of the AE are also compared to the energy associated with the injection.

Experiment

Cylindrical rock samples of Westerly granite (length 125 mm, diameter 50 mm) were loaded in a mechanical loading frame, and distilled water was injected into an axial borehole at a rate of 1 mL/min (Figure 1). 19 AE transducers were continuously recorded at a 10 MHz sample rate. Velocity

measurements were also performed periodically during the hydraulic fracturing of each sample. Automatic P-wave arrival times were used to determine AE locations with a uniform VTI velocity model. The rock samples had an axial load of 10 MPa and radial loads were applied between 12 and 30 MPa to create various differential stress conditions. After the hydraulic fracturing μ CT X-ray scans were performed to determine the fracture geometry.

Results

Figure 2 shows the resulting fracture geometry and associated AE. The hydraulic fractures are found to be predominantly a single fracture surface, with some degree of undulation, particularly at smaller differential stress. At larger differential stress, the fracture becomes more planar with a flatter surface. The AE locations cluster around the fracture and follow similar patterns to the fracture topography. A wider AE cluster is observed with the undulating surface at low differential stress, and visually narrows with the flatter fracture surface at higher differential stress. The number of AE systematically reduces with differential stress, as the fracture becomes more planar.

Here, the AE is attributed to the creation of the predominantly tensile primary fracture. Field microseismicity is often associated with

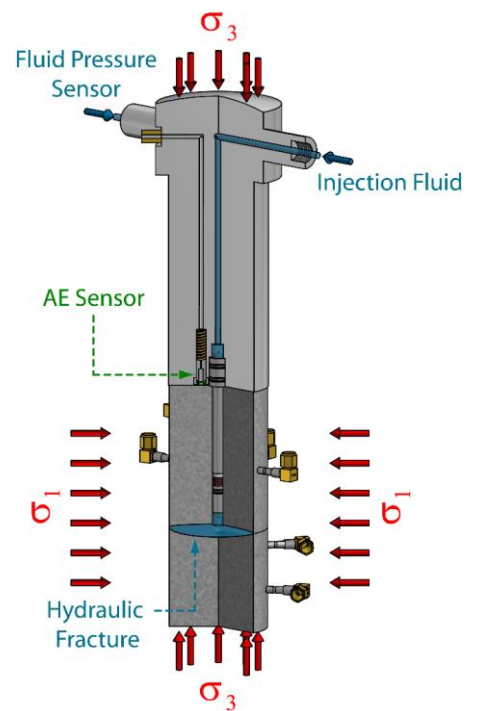


Figure 1. Schematic lab setup.

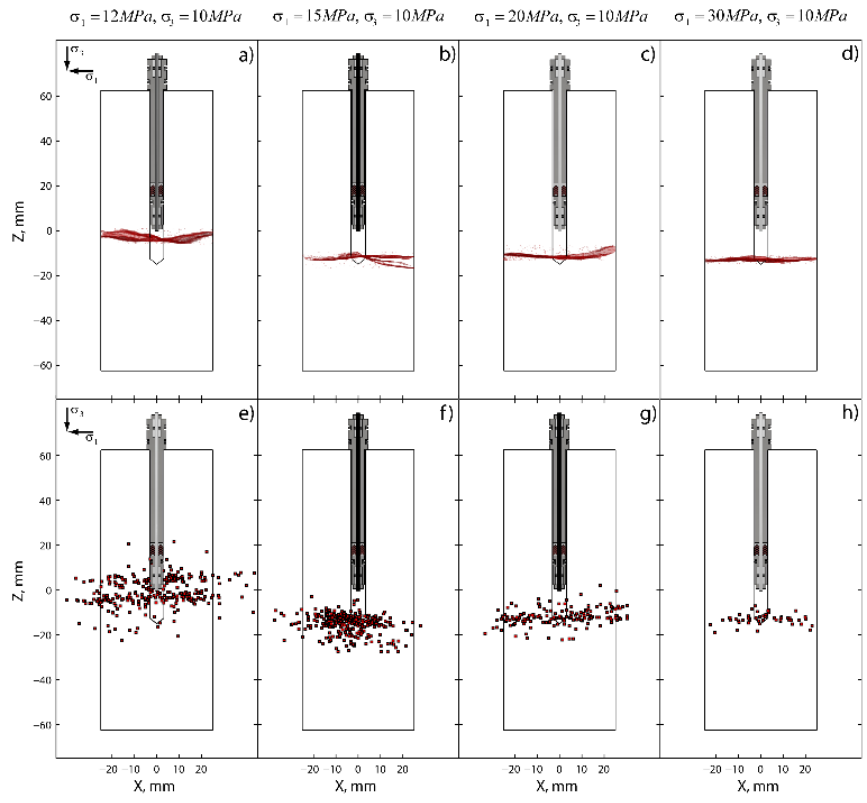


Figure 2. Four cases of hydraulic fracturing at various differential stresses, showing μ CT scans (top) and corresponding AE locations (bottom).

shearing mechanisms associated with the creation of a complex fracture network. Higher differential stress could be anticipated to result in increased rates of field microseismicity associated with higher initial shear stresses, for consistent recording sensitivity.

Acoustic Emission/Microseismic Geomechanics Model

A coupled hydraulic geomechanical model (Damjanac and Cundall, 2014) was used to simulate the hydraulic fracture. The model is based on a 'lattice' approach where springs can break and generate a new fracture. The total strain energy associated with incremental 'fracturing' in the model is used to characterize AE.

Modeling was performed for each of the rock sample experiments. The resulting fracture geometry is shown in Figure 3. The resulting fracture geometries mimic the actual fractures, with undulating fractures at low differential stress becoming more planar as the differential stress increases. Figure 4 shows the corresponding AE estimated by the model for the highest and lowest differential stress cases, again showing similar trends noted in the actual lab AE.

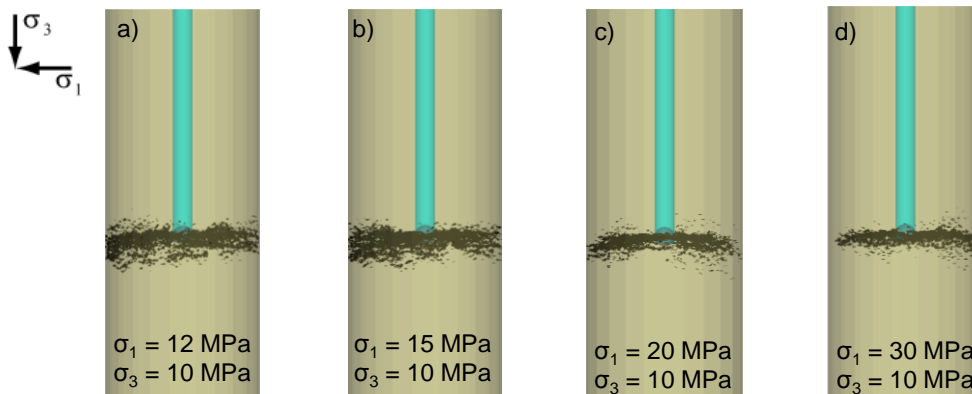


Figure 4. Geomechanical model of fracturing associated with the four scenarios.

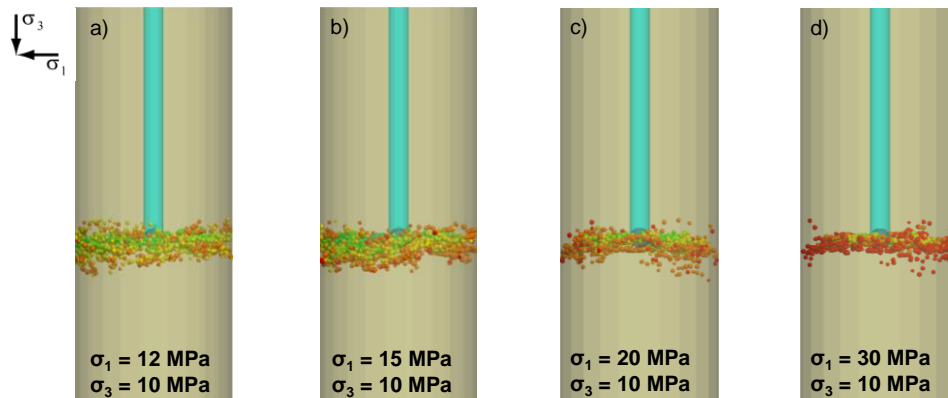


Figure 3. AE estimated by the geomechanical model, colored by time (green early, red late).

The acoustic emissions attributes can also be quantitatively compared with the geomechanical model. For example, the largest moment magnitude computed from the lab AE was approximately -7 from which a seismic energy can be estimated (e.g., Kanamori, 1978). Assuming a seismic efficiency of 0.05% for the seismic radiation component of the fracture deformation, matches the largest events from the fracturing experiments. Comparison between the resulting modeled and observed AE shows that the relative proportion of events is very similar for all the cases, i.e., the number of recorded events is consistently approximately 15% of the number of modeled events (Maxwell et al., 2016).

The seismic energy was also estimated from the AE and compared to hydraulic energy of the injection (Figure 5). The seismic energy represents a small component (less than 0.001%) of the total energy consistent with typical ratios found for microseismic monitoring of hydraulic fracturing in the field

(Maxwell, 2013). The total injection energy was also compared with the energy associated with the total axial strain of the sample (Goodfellow et al., 2015), which was a more significant component (approximately 80%). Therefore, the majority of the deformation is taking place aseismically without corresponding radiation of seismic energy that can be detected with AE monitoring.

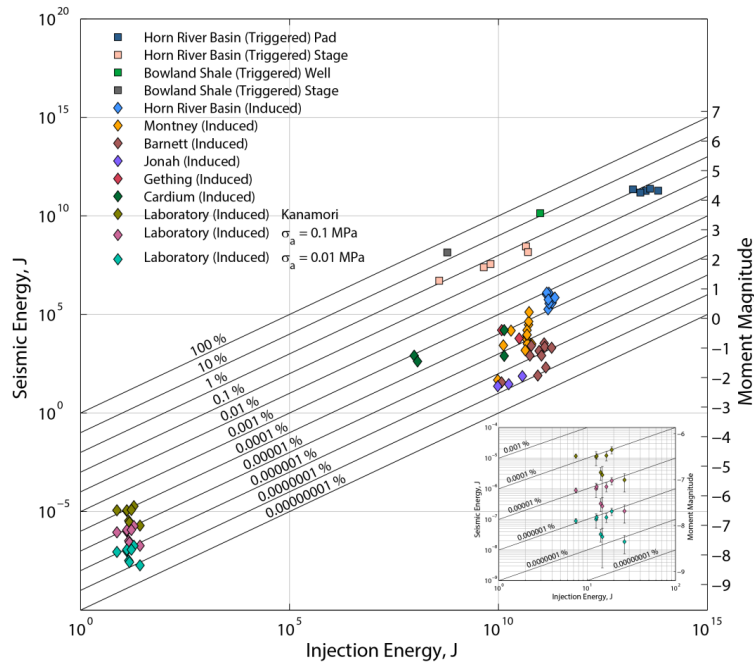


Figure 5. Comparison of seismic energy with the injection energy for laboratory AE and field microseismic (from Goodfellow et al., 2015).

Conclusions

The laboratory hydraulic fracturing demonstrated that higher differential stress produced a more planar fracture geometry. AE locations closely clustered around the hydraulic fracture, with moment magnitudes below -7. A geomechanical model of the fracture growth was able to replicate the fracture geometry and match the AE characteristics. Similar to field microseismic observations, the seismic energy was found to represent a small portion of the total hydraulic energy associated with the injection indicating that significant aseismic deformation occurs.

Acknowledgements

The authors wish to thank Laszlo Lombos (formerly of ErgoTech Ltd.) for designing the hydraulic injector system, and Farzine Nasserri (UofT) and Will Flynn (IMaGE) for their assistance conducting the experiments. Mark Mack and BT Lee assisted with the modeling.

References

- Damjanac, B., and P. Cundall, 2014, Application of distinct element methods to simulation of hydraulic fracturing in naturally fractured reservoirs, in *Recent Advances in Numerical Simulation of Hydraulic Fracture 2014*.
- Goodfellow, S. D., M. H. B. Nasserri, S. C. Maxwell, and R. P. Young, 2015, Hydraulic fracture energy budget: Insights from the laboratory, *Geophys. Res. Lett.*, 42, doi:10.1002/2015GL063093.
- Kanamori, H., 1978, Quantification of earthquakes: *Nature*, 271, 411–414, <http://dx.doi.org/10.1038/271411a0>.
- Maxwell, S. C., 2013, Unintentional seismicity induced by hydraulic fracturing, *CSEG Recorder*, 38.
- Maxwell, S.C., S. Goodfellow, B. Lee, M. Mack and R.P. Young, 2016, Acoustic Emission geomechanics characterization of laboratory hydraulic fracturing, presented at the SEG AGM in Dallas.